



# Machine learning the Kondo entanglement cloud from local measurements

Faluke Aikebaier <sup>1,2,3</sup>, Teemu Ojanen,<sup>2,3</sup> and Jose L. Lado <sup>1</sup>

<sup>1</sup>*Department of Applied Physics, Aalto University, 00076 Espoo, Finland*

<sup>2</sup>*Computational Physics Laboratory, Physics Unit, Faculty of Engineering and Natural Sciences, Tampere University, FI-33014 Tampere, Finland*

<sup>3</sup>*Helsinki Institute of Physics, P.O. Box 64, FI-00014, Finland*



(Received 20 November 2023; revised 3 April 2024; accepted 22 April 2024; published 8 May 2024)

A quantum coherent screening cloud around a magnetic impurity in metallic systems is the hallmark of the antiferromagnetic Kondo effect. Despite the central role of the Kondo effect in quantum materials, the structure of quantum correlations of the screening cloud has defied direct observations. In this work, we introduce a machine-learning algorithm that allows one to spatially map the entangled electronic modes in the vicinity of the impurity site from experimentally accessible data. We demonstrate that local correlators allow reconstruction of the local many-body correlation entropy in real space in a double Kondo system with overlapping entanglement clouds. Our machine-learning methodology allows bypassing the typical requirement of measuring long-range nonlocal correlators with conventional methods. We show that our machine-learning algorithm is transferable between different Kondo system sizes, and we show its robustness in the presence of noisy correlators. Our work establishes the potential machine-learning methods to map many-body entanglement from real-space measurements.

DOI: [10.1103/PhysRevB.109.195125](https://doi.org/10.1103/PhysRevB.109.195125)

## I. INTRODUCTION

Strongly interacting quantum many-body systems exhibit a wealth of intricate physical phenomena. Quantum impurity problems, and in particular the Kondo problem [1–3], play a crucial role in capturing properties of the localized interactions within a larger quantum system [4–6]. Such systems provide a paradigmatic framework for understanding the correlation effects and related entanglement features in many-body systems [7–10]. A hallmark feature of the Kondo effect is the formation of a dynamic cloud of conduction electrons, or “the Kondo screening cloud,” surrounding the impurity. The Kondo cloud, which plays a crucial role in understanding the Kondo problem [11], leads to electron entanglement at mesoscopic scales [12,13]. Recent experiments have directly confirmed the existence of the Kondo screening cloud [14]; however, the detailed structure of the quantum many-body correlations remains elusive. Correlation effects are essential for understanding the emergence of the Kondo effect and the subsequent formation of the Kondo screening cloud [12,15–18], motivating the development of more powerful strategies to imaging the Kondo entanglement cloud.

Entanglement properties of quantum materials are remarkably challenging to extract in experiments. From a theory perspective, correlations in electronic systems can be quantified by means of the von Neumann entropy obtained from a one-particle density matrix, known as the correlation entropy [19–24], a quantity that vanishes for any noninteracting electronic system. Experimental measurement of the correlation entropy is greatly challenging as it requires knowledge of all correlators in the whole system [25–27]. The machine-learning methodologies algorithm offers a potential alternative strategy for extracting the correlation entropy

from a reduced set of measurements [28]. Machine-learning methods have been demonstrated to be highly successful in extracting Hamiltonians from experimental data [29–39], and for automatic tuning of quantum systems without human intervention [40–47]. However, its potential for extracting local entanglement properties in homogeneous single-impurity Kondo problems remains relatively unexplored.

In this work, we develop a machine-learning assisted algorithm, which employs local measurements near a Kondo magnetic impurity to predict the spatial entanglement in real space. We demonstrate that a supervised machine-learning approach allows one to predict the spatially varying correlation entropy density solely from local correlations. This method enables one to extract the spatial structure of the quantum correlations in the Kondo screening cloud, as well as the overlap between two Kondo screening clouds created by two Kondo impurities. We demonstrate this methodology in the presence of noisy data, showing the potential of our approach in an experimentally realistic scenario. This paper is organized as follows. In Sec. II, we introduce the Kondo impurity model and the formulation of correlation entropy density. In Sec. III, we analyze the developed machine-learning methodology to predict the correlation entropy density from measurable local correlators, including its transferability and the impact of noise. Finally, in Sec. IV, we summarize our conclusions.

## II. MODEL

We consider the setup shown in Fig. 1(a). Two interacting Kondo spins are coupled to the opposite sides of a noninteracting electron gas through Kondo coupling. These couplings induce many-body correlations along the noninteracting gas, at a length scale determined by the Kondo cloud length, and

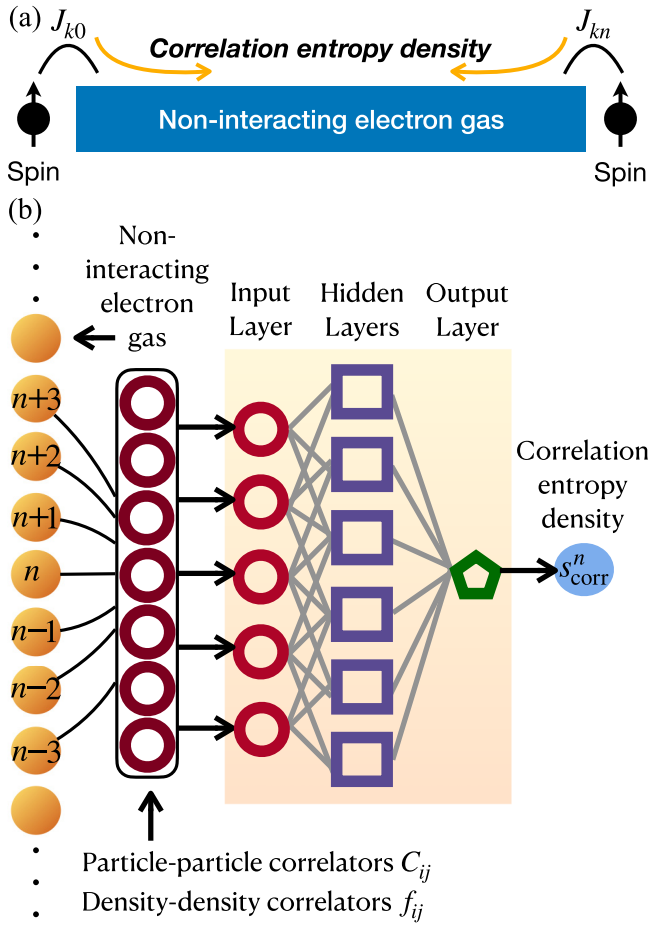


FIG. 1. (a) Schematic of the model. Two interacting spins on the two sides of the noninteracting chain induces many-body correlation via Kondo coupling. (b) Schematic of the workflow of the neural-network model, taking as input spatially resolved local correlators, and providing as output the spatial profile of the correlation entropy density.

when the Kondo clouds overlap, they lead to entanglement between distant Kondo sites. The Hamiltonian of the setup is written as follows:

$$\begin{aligned}
 H = & \left[ J_{k0} \mathbf{S}_0 \cdot \mathbf{s}_1 + U \left( \hat{n}_{0\uparrow} - \frac{1}{2} \right) \left( \hat{n}_{0\downarrow} - \frac{1}{2} \right) \right] \\
 & - t \sum_{j=1, \sigma}^{n-1} (c_{j\sigma}^\dagger c_{j+1\sigma} + \text{H.c.}) + \mu \sum_{j=1, \sigma}^{n-1} c_{j\sigma}^\dagger c_{j\sigma} \\
 & + t' \sum_{j=1, \sigma}^{n-1} (c_{j\sigma}^\dagger c_{j+2\sigma} + \text{H.c.}) + \left[ J_{kn} \mathbf{s}_n \cdot \mathbf{S}_{n+1} \right. \\
 & \left. + U \left( \hat{n}_{n+1, \uparrow} - \frac{1}{2} \right) \left( \hat{n}_{n+1, \downarrow} - \frac{1}{2} \right) \right], \quad (1)
 \end{aligned}$$

where  $c_{j\sigma}^{(\dagger)}$  is the annihilation (creation) operator at site  $j$  with spin  $\sigma$ , and  $\hat{n}_{j\sigma}$  is the density operator at site  $j$  with spin  $\sigma$ . For the interacting terms,  $J_{k0}$  and  $J_{kn}$  are the Kondo coupling strengths,  $U$  is the on-site interaction to induce charge localization in the Kondo site,  $\mathbf{S}_{0,n+1}$  is the spin-1/2 operator, and  $\mathbf{s}_{1,n}$  is the local spin operator of the noninteracting

chain. For the noninteracting chain, we consider nearest- and next-nearest-neighbor hopping  $t$  and  $t'$ , and the chemical potential  $\mu$ . We will focus on values of the Kondo couplings corresponding to Kondo clouds smaller than the size of the noninteracting electron gas to minimize finite-size effects.

To characterize the entanglement, we employ the one-particle density matrix, also known as the correlation matrix [19–21]. It provides information about the distribution of electrons and their correlations in the system [48–51], and is defined as

$$C_{ij}^{ss'} = \langle \Psi_0 | c_{is}^\dagger c_{js'} | \Psi_0 \rangle, \quad (2)$$

where  $|\Psi_0\rangle$  refers to a fermionic many-body state. Its eigensolutions offer crucial information about the correlation effect in the many-body state. The eigenvectors  $v_k$  define a set of natural orbitals [52,53], and the corresponding eigenvalues  $0 \leq \alpha_k \leq 1$  are their ground-state occupation numbers. The existence of natural orbitals with eigenvalues  $0 < \alpha_k < 1$  signifies electronic entanglement. Filled and empty orbitals are associated with occupation numbers of 1 and 0, and these orbitals do not contribute to the mode entanglement. In the Kondo impurity models, despite the near-macroscopic reorganization of the Fermi sea, the entanglement in the Kondo problem has a few-body character with only a handful of natural orbitals with eigenvalues that significantly differ from 0 and 1 [54–56]. Considering the spatial feature of the induced correlation, we define the correlation entropy density as follows:

$$s_{\text{corr}}(\mathbf{r}) = - \sum_k (\alpha_k \ln \alpha_k) |v_k|^2(\mathbf{r}), \quad (3)$$

where  $\alpha_k$  are the eigenvalues and the  $v_k$  are the corresponding eigenvectors of the one-body density matrix. The full correlation entropy can be determined by integrating over the correlation entropy density  $s_{\text{corr}}$  through the entire fermionic chain. The correlation entropy density serves as a valuable tool for understanding the interaction-induced many-particle correlations within the system. In the absence of particle-particle interactions, all the natural orbitals are either completely filled or empty, and the correlation entropy density  $s_{\text{corr}}$  vanishes. The orbitals with fractional population give rise to a finite  $s_{\text{corr}}$ , which also encode the spatial structure of the correlations through  $v_k$ .

The correlation entropy density  $s_{\text{corr}}$  of a 20-site fermionic chain, with 18-site noninteracting sites, is shown in Fig. 2. The ground state of such a chain is determined by using the tensor-network matrix-product state formalism [57–61], which allows extraction of the different particle-particle correlators in the full system and evaluation of the correlation entropy density. The correlation entropy density with one interacting spin for various strengths of the coupling constant  $J_{k0}$  is shown in Fig. 2(a). We can see that  $s_{\text{corr}}$  is strongest at the interacting spin site, and gradually reduces towards the center of the noninteracting chain. The oscillation of  $s_{\text{corr}}$  originates from the oscillation of the particle-particle correlators within a scale of the order of the Fermi wavelength. The horizontal and vertical cuts of Fig. 2(a) for specific values of  $J_{k0}$  and for specific sites are shown in Figs. 2(c) and 2(e) separately.

For the case of two interacting spins, the correlation entropy density  $s_{\text{corr}}$  for various strengths of the coupling

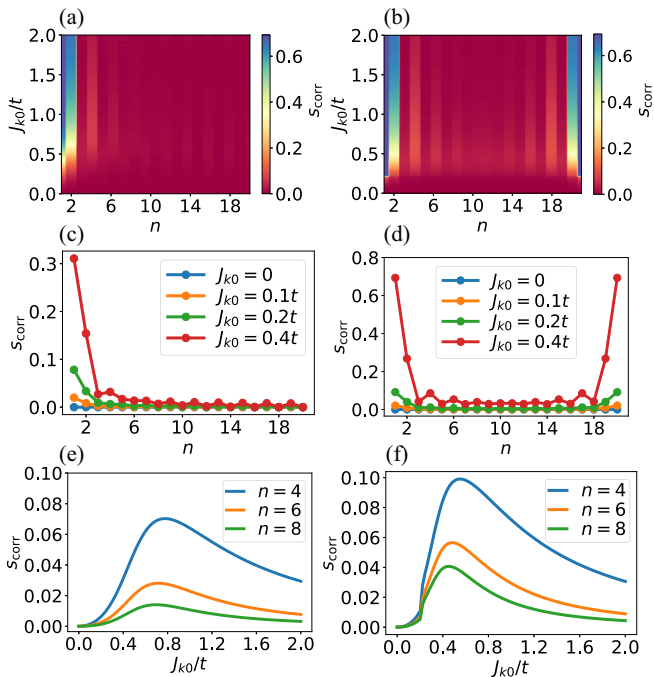


FIG. 2. Correlation entropy density  $s_{\text{corr}}$  of a 20-site (noninteracting 18-site) model. (a) A heat plot for the case of the interacting spin is located on the left of the noninteracting chain. (b) A heat plot for the case of two interacting spins (with coupling constant  $J_{k0} = J_{kn}$ ) is located on the two sides of the noninteracting chain. (c) Examples of (a) for specific values of the coupling constant  $J_{k0}$ . (d) Examples of (b) for specific values of the coupling constant  $J_{k0}$ . (e) Dependence of  $s_{\text{corr}}$  on  $J_{k0}$  at different sites in the case of a single interacting spin. (f) Dependence of  $s_{\text{corr}}$  on  $J_{k0} = J_{kn}$  at different sites in the case of two interacting spins.

constant is shown in Figs. 2(b), 2(d) and 2(f). As one can see, the correlation induced by the other interacting spin brings changes to the profile of  $s_{\text{corr}}$ . Two sources of correlation in the noninteracting chain enhance  $s_{\text{corr}}$  throughout the chain. The decay of  $s_{\text{corr}}$  towards the center of the noninteracting chain is also slower than the case of a single interacting spin. As the correlation entropy represents the complexity of the correlation, the case of two interacting spins could provide more insights for the quantum entanglement in such systems.

### III. MACHINE-LEARNING CORRELATION ENTROPY DENSITY

#### A. Local prediction of the correlation density

We first note that the straightforward experimental extraction of the correlation entropy density  $s_{\text{corr}}$  requires measurement of all the particle-particle correlators. For an  $n$ -site system, the number of associated correlators is  $2n^2$  including long-range ones, a greatly challenging task for large systems. This limitation can be bypassed by directly using a machine-learning model to extract the correlation entropy from a reduced set of local correlators. In particular, we extract particle-particle correlators related to each specific site by providing local correlators of the three sites around each location (see the Appendix for details) [62]. At first glance,

such an approach leads to a significant information loss, as all the nonlocal correlations required to extract the correlation entropy are lost. This information loss is compensated by providing the local density-density correlators,

$$f_{ij}^{ss'} = \langle \Psi_0 | n_{is} n_{js'} | \Psi_0 \rangle, \quad (4)$$

of the three neighboring sites. The inclusion of density-density correlators provides further information that the conventional calculation of the correlation entropy does not have access to, but that our machine-learning algorithm can exploit to reconstruct the correlation entropy. We will show that these local particle-particle and density-density correlators are enough to train a supervised learning algorithm to predict the related correlation entropy density.

As an input, our algorithm assumes correlators around one site and outputs the entropy density at that site. The training data for the machine-learning model are generated according to the following prescription. Solving the Hamiltonian in Eq. (1) with randomly generated tight-binding parameters ( $t'$ ,  $\mu$ ,  $J_{k0}$ , and  $J_{kn}$ ) for a 32-site model enables us to compute the correlation entropy density in Eq. (3), which is the quantity to be predicted by the algorithm, exactly at each site. The input of the machine-learning algorithm could be obtained by measuring the relevant particle-particle correlators in Eq. (2) and density-density correlators in Eq. (4). The input correlators of the algorithms correspond to the average between the  $n$ th preceding and subsequent sites around a specific site of the fermionic chain.<sup>1</sup> This leads to a 32-dimensional entry for predicting the correlation entropy density. We collected 40 000 examples for training purposes (see the Appendix for details). The examples are generated with the following ranges of the tight-binding parameters:  $J_{k0}, J_{kn} \in [0, 2t]$ ,  $\mu \in [0, 2t]$ ,  $t' \in [0, t]$ . We use a principal component analysis [63], keeping all components, to transform the data to an uncorrelated basis. For training purposes, we use the Box-Cox transformation [64] to reduce the potential large relative errors created from the small values of  $s_{\text{corr}}$ . With the transformed dataset, we develop the neural-network structure containing 12 hidden layers with 512 nodes, as shown in Fig. 1(b).

The comparison between the predicted and the actual values of  $s_{\text{corr}}$  is shown in Fig. 3(a). The mean absolute error (MAE) of the model is 0.001. The trained algorithm allows us to predict the correlation entropy density at any site of a model for any sets of tight-binding parameters. In Fig. 3(b), the MAE is shown for each site of the fermionic chain for four random fermionic chains. The error values remain at the same levels for the majority sites. The prediction of each site of four random fermionic chains is shown in Fig. 3(c) in logarithmic scale and Fig. 3(d) in the original scale. As can be seen, the predictions match very well with the values of  $s_{\text{corr}}$ .

#### B. Transfer learning to various-size Kondo models

In the following, we show how an algorithm training on a specific system size allows one to make a prediction for

<sup>1</sup>For edge sites the average is replaced for the single existing  $n$ th neighbor.

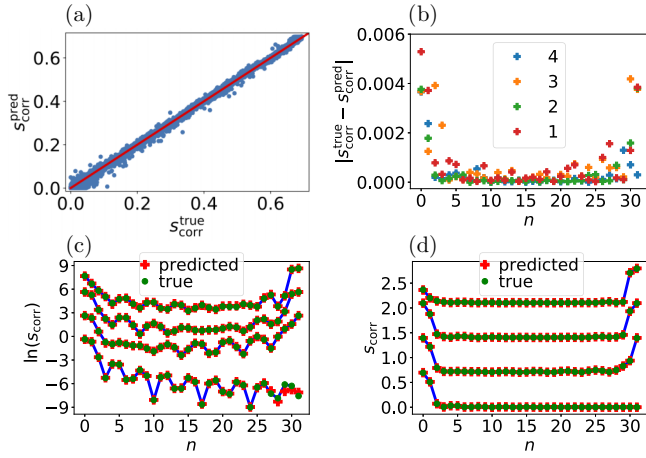


FIG. 3. (a) Comparison between predicted and actual values of  $s_{\text{corr}}$ . (b) Mean absolute error of  $s_{\text{corr}}$  on each site of four random fermionic chains. (c) Prediction on each site of the entire 32-site chain of  $s_{\text{corr}}$  in logarithmic scale for the four fermionic chains in (b). (d) Prediction on each site of the entire 32-site chain of  $s_{\text{corr}}$  for the four fermionic chains in (b). Curves in (c) and (d) are shifted along the vertical axis for clarity.

Kondo models of other systems sizes. The trained neural-network model uses local correlators to predict the correlation entropy density  $s_{\text{corr}}$ . For a random site, the relevant correlators are only associated with the preceding and subsequent three sites, meaning that the machine-learning methodology is local by definition. The model was trained before on a 32-site fermionic chain, but for larger and smaller chains, the relevant correlators are expected to show an analogous phenomenology for larger and smaller chains. This built-in locality in the machine-learning algorithm motivates analyzing the potential transferability of the neural-network model. For this purpose, we directly evaluate the trained neural-network model to predict  $s_{\text{corr}}$  on a larger or smaller fermionic chain. We apply the trained neural-network model on 24-, 28-, 36-, and 40-site fermionic chains, each consisting of 5000 randomly generated examples.

The site-specific MAE for  $s_{\text{corr}}$  of the fermionic chains with different sizes is shown in Fig. 4(a). The size-specific MAE for  $s_{\text{corr}}$  of the fermionic chains at different sites is shown in Fig. 4(b). As can be seen, the average MAE gradually increases for the larger and smaller fermionic chains, but it remains in the error range of the 32-site fermionic chain. Hence, the prediction is reliable for fermionic chains with different sizes.

The accuracy of the model can also be examined by fidelity defined as

$$\mathcal{F} = \frac{|\langle s_{\text{corr}}^{\text{pred}} \cdot s_{\text{corr}}^{\text{true}} \rangle - \langle s_{\text{corr}}^{\text{pred}} \rangle \cdot \langle s_{\text{corr}}^{\text{true}} \rangle|}{\sqrt{[\langle (s_{\text{corr}}^{\text{true}})^2 \rangle - \langle s_{\text{corr}}^{\text{true}} \rangle^2][\langle (s_{\text{corr}}^{\text{pred}})^2 \rangle - \langle s_{\text{corr}}^{\text{pred}} \rangle^2]}}. \quad (5)$$

The previous quantity factors out the impact of different magnitudes for the correlation entropy when computing the error, leading to  $\mathcal{F} = 1$  if the prediction of the machine-learning algorithm is flawless and  $\mathcal{F} = 0$  if the algorithm does not have predictive power. The fidelity for different system sizes and sites is plotted in Figs. 4(c) and 4(d), respectively. We

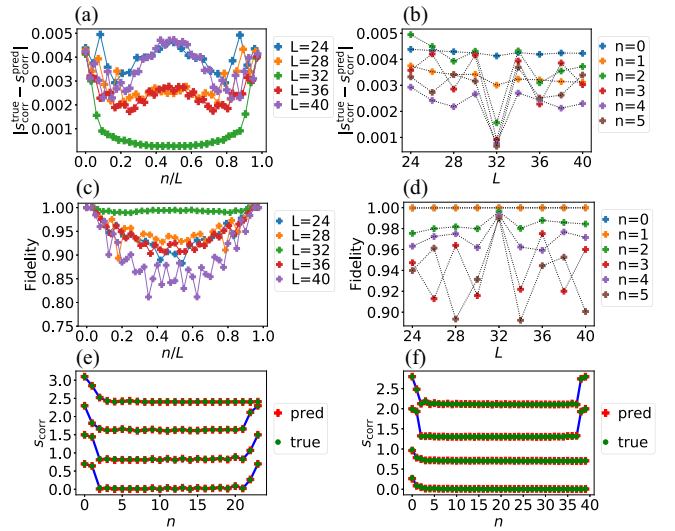


FIG. 4. Site-specific (a) absolute error and (c) fidelity of the prediction of the neural-network model on fermionic chains with different sizes. Size-specific (b) absolute error and (d) fidelity of the prediction of the neural-network model on different sites of the fermionic chains. Comparison of the actual and predicted values on the (e) 24-site fermionic chain and (f) 40-site fermionic chain. For clarity, the curves are shifted along the vertical axis in (e) and (f).

observe that the fidelity of the larger and smaller chains also remains in the same range, despite the algorithm not having been trained in those systems, and the neural-network model is reliable on predicting different sizes of chains. As specific examples, the prediction of the each site of four random examples of 24- and 40-site chains is shown in Figs. 4(e) and 4(f) separately. The small departures in the transfer learning can be associated to slightly different finite-size effects in the different systems. Overall, these results demonstrate that a machine-learning algorithm of the correlation entropy based on local correlators is transferable between different systems sizes, further supporting the fact that the correlation entropy can be determined locally.

### C. Resilience to noise

In real experimental data, the extracted correlators may contain a certain amount of noise. For this purpose, we now address the robustness of the neural-network model by including random numerical noise in the data.

We denote the particle-particle and density-density correlators as  $\Lambda_{ij}^{ss',0} = \{C_{ij}^{ss'}, f_{ij}^{ss'}\}$ , and introduce the noise in the correlators as

$$\Lambda_{ij}^{ss'} = \Lambda_{ij}^{ss',0} + \chi_{ij}^{ss'}, \quad (6)$$

where  $\chi_{ij}^{ss'}$  is the random noise between  $[-\omega, \omega]$ , and  $\omega$  controls the amplitude of the noise. The neural-network model is trained on the 32-site fermionic chain for various degrees of noise and tested for 5000 randomly generated fermionic chains. The MAE and the fidelity are shown in Fig. 5(a) and Fig. 5(b), respectively. It is observed that while the prediction of the correlation entropy close to the Kondo impurity is relatively robust, prediction of the correlation entropy density

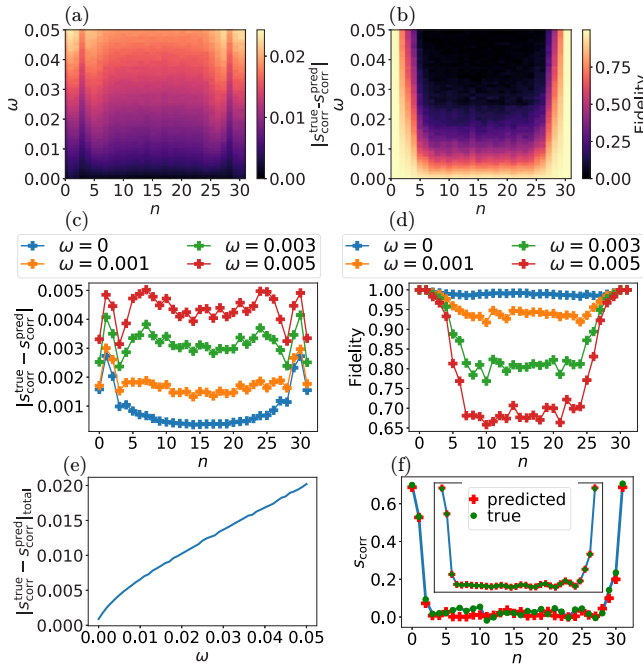


FIG. 5. Effect of numerical noise on the prediction of the correlation entropy density trained on the 32-site fermionic chain. (a) Site-specific MAE of the correlation entropy density for various values of the noise rate  $\omega$ . (b) Site-specific fidelity of the correlation entropy density for various values of the noise rate  $\omega$ . (c) Horizontal cuts from (a) for smaller values of  $\omega$ . (d) Horizontal cuts from (b) for smaller values of  $\omega$ . (e) Total MAE as a function of the noise rate  $\omega$ . (f) A comparison between actual and predicted values of  $s_{\text{corr}}$  for larger values of  $\omega = 0.05$  and  $\omega = 0$  (inset).

far from the impurity requires accurate measurements of the correlators. The error in the correlation density for specific values of  $\omega < 0.01$  is shown in Fig. 5(c), and its associated fidelity in Fig. 5(d). Analogous to Figs. 5(a) and 5(b), it is observed that the entropy around the Kondo impurity can be predicted accurately, whereas far from it the existence of noise decreases the fidelity of the prediction. The total MAE as a function of  $\omega$  is shown in Fig. 5(e), where it is observed that the error increases approximately linearly with the noise level. As a reference, we show a comparison between the true and predicted  $s_{\text{corr}}$  for  $\omega = 0.05$  and  $\omega = 0$  in Fig. 5(f). Our results suggest that predicting the correlation entropy featuring low levels of correlation requires precise correlator data. In contrast, predictions of the entropy close to the impurities, which in our calculation corresponds to a length comparable to the Kondo cloud, are robust to the presence of noise.

#### IV. CONCLUSION

In this work, we demonstrated that a machine-learning algorithm, assuming local correlators as an input, can accurately predict the many-body entanglement structure of a Kondo screening cloud as characterized by the correlation entropy. Our methodology combines local single-particle and density correlators, showing that these quantities contain enough information to reconstruct the correlation entropy in real space. Our method demonstrates that machine learning allows

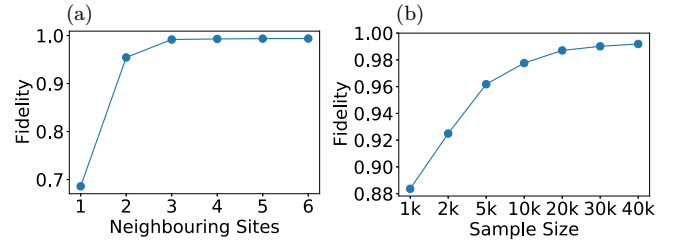


FIG. 6. (a) Fidelity of the neural-network model as a function of the nearest-neighbor sites considered in the training. The maximum sample size of 40 000 is used in each case. It is observed that considering correlators in three neighboring sites provides high-quality predictions. (b) Fidelity of the neural-network model as a function of the sample size of the training data; the correlators are extracted from three neighboring sites. It is observed that the accuracy of the algorithm saturates at approximately 20 000 samples.

bypassing the need to obtain long-range correlators required for direct methods. We showed that owing to the local nature of the input data, our algorithm is transferable to different system sizes. Thus, our methodology can be applied to systems not included in the training set. Finally, we demonstrated the resilience of our algorithm to noise, showing that the correlation entropy is reasonably robust in the presence of sizable inaccuracies in the measured correlators. The extraction of real-space entanglement offers valuable insight into the intricate interplay of correlations within the system, including the determination of a spatial profile of the Kondo cloud. Our results establish the potential of machine-learning methods to reveal entanglement in many-body systems, including spatially inhomogeneous quantum materials.

#### ACKNOWLEDGMENTS

F.A. acknowledges the financial support from the Magnus Ehrnrooth Foundation. T.O. acknowledges the Academy of Finland Project No. 331094 for support. J.L.L. acknowledges the financial support from the Academy of Finland Projects No. 331342 and No. 358088 and the Jane and Aatos Erkko Foundation. F.A. and J.L.L. acknowledge the computational resources provided by the Aalto Science-IT project.

#### APPENDIX: CHOICE OF LOCAL CORRELATORS AND SAMPLE SIZE

Here, we address the accuracy of our algorithm as a function of the number of neighboring sites from which correlators were extracted, and the sample size of the training set.

Figure 6(a) shows the fidelity  $\mathcal{F}$  of the neural-network model trained on correlators extracted from various numbers of neighboring sites surrounding a given internal site of the noninteracting chain. As it is observed, the accuracy of the model is much lower for neighboring sites of less than three, and improves as the number of neighboring sites is increased. Increasing the number of included correlators significantly increases the number of correlators that must be determined. We find that satisfactory accuracy is attained with correlators

extracted from three neighboring sites, and therefore we focus on the three-neighbor case for training the optimal neural-network model.

Figure 6(b) shows the fidelity of the neural-network model as a function of the size of the training set. As it is observed, the accuracy of the model increases as the size of the training set increases. We find that the accuracy of the model saturates for sample sizes larger than 20 000. Our calculations are

therefore in the regime where the training data is large enough to saturate the accuracy of the algorithm.

Given the behavior described above, we focus the results of our manuscript on a training set with 40 000 examples, where the correlators are extracted from three neighboring sites. This choice enables a modest number of correlators to be determined, while maintaining satisfactory accuracy of the neural-network model.

- 
- [1] W. de Haas, J. de Boer, and G. van den Berg, The electrical resistance of gold, copper and lead at low temperatures, *Physica* **1**, 1115 (1934).
- [2] J. Kondo, Resistance minimum in dilute magnetic alloys, *Prog. Theor. Phys.* **32**, 37 (1964).
- [3] N. Andrei, K. Furuya, and J. H. Lowenstein, Solution of the Kondo problem, *Rev. Mod. Phys.* **55**, 331 (1983).
- [4] A. C. Hewson, *The Kondo Problem to Heavy Fermions* (Cambridge University Press, Cambridge, 1993).
- [5] O. Újsághy, J. Kroha, L. Szunyogh, and A. Zawadowski, Theory of the Fano resonance in the STM tunneling density of states due to a single Kondo impurity, *Phys. Rev. Lett.* **85**, 2557 (2000).
- [6] N. Knorr, M. A. Schneider, L. Diekhöner, P. Wahl, and K. Kern, Kondo effect of single Co adatoms on Cu surfaces, *Phys. Rev. Lett.* **88**, 096804 (2002).
- [7] S. Y. Cho and R. H. McKenzie, Quantum entanglement in the two-impurity Kondo model, *Phys. Rev. A* **73**, 012109 (2006).
- [8] I. Affleck, N. Laflorencie, and E. S. Sørensen, Entanglement entropy in quantum impurity systems and systems with boundaries, *J. Phys. A: Math. Theor.* **42**, 504009 (2009).
- [9] S. Wirth and F. Steglich, Exploring heavy fermions from macroscopic to microscopic length scales, *Nat. Rev. Mater.* **1**, 16051 (2016).
- [10] H. Tsunetsugu, M. Sigrist, and K. Ueda, The ground-state phase diagram of the one-dimensional Kondo lattice model, *Rev. Mod. Phys.* **69**, 809 (1997).
- [11] A. Mukherjee, A. Mukherjee, N. S. Vidhyadhiraja, A. Taraphder, and S. Lal, Unveiling the Kondo cloud: Unitary renormalization-group study of the Kondo model, *Phys. Rev. B* **105**, 085119 (2022).
- [12] V. Barzykin and I. Affleck, The Kondo screening cloud: What can we learn from perturbation theory? *Phys. Rev. Lett.* **76**, 4959 (1996).
- [13] I. Affleck, The Kondo screening cloud: What it is and how to observe it, in *Perspectives of Mesoscopic Physics* (World Scientific, Singapore, 2010), pp. 1–44.
- [14] I. V. Borzenets, J. Shim, J. C. H. Chen, A. Ludwig, A. D. Wieck, S. Tarucha, H.-S. Sim, and M. Yamamoto, Observation of the Kondo screening cloud, *Nature (London)* **579**, 210 (2020).
- [15] J. E. Gubernatis, J. E. Hirsch, and D. J. Scalapino, Spin and charge correlations around an anderson magnetic impurity, *Phys. Rev. B* **35**, 8478 (1987).
- [16] V. Barzykin and I. Affleck, Screening cloud in the  $k$ -channel Kondo model: Perturbative and large- $k$  results, *Phys. Rev. B* **57**, 432 (1998).
- [17] L. Borda, Kondo screening cloud in a one-dimensional wire: Numerical renormalization group study, *Phys. Rev. B* **75**, 041307(R) (2007).
- [18] A. Holzner, I. P. McCulloch, U. Schollwöck, J. von Delft, and F. Heidrich-Meisner, Kondo screening cloud in the single-impurity Anderson model: A density matrix renormalization group study, *Phys. Rev. B* **80**, 205114 (2009).
- [19] R.-Q. He and Z.-Y. Lu, Quantum renormalization groups based on natural orbitals, *Phys. Rev. B* **89**, 085108 (2014).
- [20] Y. Lu, M. Höppner, O. Gunnarsson, and M. W. Haverkort, Efficient real-frequency solver for dynamical mean-field theory, *Phys. Rev. B* **90**, 085102 (2014).
- [21] M. T. Fishman and S. R. White, Compression of correlation matrices and an efficient method for forming matrix product states of fermionic Gaussian states, *Phys. Rev. B* **92**, 075132 (2015).
- [22] R. O. Esquivel, A. L. Rodríguez, R. P. Sagar, M. Hô, and V. H. Smith, Physical interpretation of information entropy: Numerical evidence of the collins conjecture, *Phys. Rev. A* **54**, 259 (1996).
- [23] P. Gersdorf, W. John, J. P. Perdew, and P. Ziesche, Correlation entropy of the  $\text{H}_2$  molecule, *Int. J. Quantum Chem.* **61**, 935 (1997).
- [24] P. Ziesche, O. Gunnarsson, W. John, and H. Beck, Two-site Hubbard model, the Bardeen-Cooper-Schrieffer model, and the concept of correlation entropy, *Phys. Rev. B* **55**, 10270 (1997).
- [25] Z. Huang, H. Wang, and S. Kais, Entanglement and electron correlation in quantum chemistry calculations, *J. Mod. Opt.* **53**, 2543 (2006).
- [26] C. L. Benavides-Riveros, N. N. Lathiotakis, C. Schilling, and M. A. L. Marques, Relating correlation measures: The importance of the energy gap, *Phys. Rev. A* **95**, 032507 (2017).
- [27] D. L. B. Ferreira, T. O. Maciel, R. O. Vianna, and F. Iemini, Quantum correlations, entanglement spectrum, and coherence of the two-particle reduced density matrix in the extended Hubbard model, *Phys. Rev. B* **105**, 115145 (2022).
- [28] F. Aikebaier, T. Ojanen, and J. L. Lado, Extracting electronic many-body correlations from local measurements with artificial neural networks, *SciPost Phys. Core* **6**, 030 (2023).
- [29] S. G. Schirmer and D. K. L. Oi, Two-qubit Hamiltonian tomography by Bayesian analysis of noisy data, *Phys. Rev. A* **80**, 022333 (2009).
- [30] J. Wang, S. Paesani, R. Santagati, S. Knauer, A. A. Gentile, N. Wiebe, M. Petruzzella, J. L. O'Brien, J. G. Rarity, A. Laing, and M. G. Thompson, Experimental quantum Hamiltonian learning, *Nat. Phys.* **13**, 551 (2017).
- [31] I. Hincks, C. Granade, and D. G. Cory, Statistical inference with quantum measurements: Methodologies for nitrogen vacancy centers in diamond, *New J. Phys.* **20**, 013022 (2018).
- [32] N. Karjalainen, Z. Lippo, G. Chen, R. Koch, A. O. Fumega, and J. L. Lado, Hamiltonian inference from dynamical excitations

- in confined quantum magnets, *Phys. Rev. Appl.* **20**, 024054 (2023).
- [33] M. Khosravian, R. Koch, and J. L. Lado, Hamiltonian learning with real-space impurity tomography in topological moiré superconductors, *J. Phys.: Mater.* **7**, 015012 (2024).
- [34] A. Valenti, G. Jin, J. Léonard, S. D. Huber, and E. Greplova, Scalable Hamiltonian learning for large-scale out-of-equilibrium quantum dynamics, *Phys. Rev. A* **105**, 023302 (2022).
- [35] L. Che, C. Wei, Y. Huang, D. Zhao, S. Xue, X. Nie, J. Li, D. Lu, and T. Xin, Learning quantum Hamiltonians from single-qubit measurements, *Phys. Rev. Res.* **3**, 023246 (2021).
- [36] A. Valenti, E. van Nieuwenburg, S. Huber, and E. Greplova, Hamiltonian learning for quantum error correction, *Phys. Rev. Res.* **1**, 033092 (2019).
- [37] R. Koch and J. L. Lado, Designing quantum many-body matter with conditional generative adversarial networks, *Phys. Rev. Res.* **4**, 033223 (2022).
- [38] C. Di Franco, M. Paternostro, and M. S. Kim, Hamiltonian tomography in an access-limited setting without state initialization, *Phys. Rev. Lett.* **102**, 187203 (2009).
- [39] R. Koch, D. van Driel, A. Bordin, J. L. Lado, and E. Greplova, Adversarial Hamiltonian learning of quantum dots in a minimal Kitaev chain, *Phys. Rev. Appl.* **20**, 044081 (2023).
- [40] T. Schmale, M. Reh, and M. Gärtner, Efficient quantum state tomography with convolutional neural networks, *npj Quantum Inf.* **8**, 115 (2022).
- [41] M. Neugebauer, L. Fischer, A. Jäger, S. Czischek, S. Jochim, M. Weidemüller, and M. Gärtner, Neural-network quantum state tomography in a two-qubit experiment, *Phys. Rev. A* **102**, 042604 (2020).
- [42] G. Torlai, G. Mazzola, J. Carrasquilla, M. Troyer, R. Melko, and G. Carleo, Neural-network quantum state tomography, *Nat. Phys.* **14**, 447 (2018).
- [43] Y. Quek, S. Fort, and H. K. Ng, Adaptive quantum state tomography with neural networks, *npj Quantum Inf.* **7**, 105 (2021).
- [44] A. M. Palmieri, E. Kovlakov, F. Bianchi, D. Yudin, S. Straupe, J. D. Biamonte, and S. Kulik, Experimental neural network enhanced quantum tomography, *npj Quantum Inf.* **6**, 20 (2020).
- [45] S. Ahmed, C. Sánchez Muñoz, F. Nori, and A. F. Kockum, Quantum state tomography with conditional generative adversarial networks, *Phys. Rev. Lett.* **127**, 140502 (2021).
- [46] D. Koutný, L. Motka, Z. Hradil, J. Řeháček, and L. L. Sánchez-Soto, Neural-network quantum state tomography, *Phys. Rev. A* **106**, 012409 (2022).
- [47] P. Cha, P. Ginsparg, F. Wu, J. Carrasquilla, P. L. McMahon, and E.-A. Kim, Attention-based quantum tomography, *Mach. Learn.: Sci. Technol.* **3**, 01LT01 (2022).
- [48] H. Wang and S. Kais, Quantum entanglement and electron correlation in molecular systems, *Isr. J. Chem.* **47**, 59 (2007).
- [49] M. C. Tichy, F. Mintert, and A. Buchleitner, Essential entanglement for atomic and molecular physics, *J. Phys. B: At., Mol. Opt. Phys.* **44**, 192001 (2011).
- [50] T. S. Hofer, On the basis set convergence of electron–electron entanglement measures: helium-like systems, *Front. Chem.* **1**, 24 (2013).
- [51] R. O. Esquivel, S. López-Rosa, and J. S. Dehesa, Correlation energy as a measure of non-locality: Quantum entanglement of helium-like systems, *Europhys. Lett.* **111**, 40009 (2015).
- [52] P.-O. Löwdin, Quantum theory of many-particle systems. I. Physical interpretations by means of density matrices, natural spin-orbitals, and convergence problems in the method of configurational interaction, *Phys. Rev.* **97**, 1474 (1955).
- [53] P. E. M. Siegbahn, J. Almlöf, A. Heiberg, and B. O. Roos, The complete active space SCF (CASSCF) method in a Newton–Raphson formulation with application to the HNO molecule, *J. Chem. Phys.* **74**, 2384 (1981).
- [54] C. Yang and A. E. Feiguin, Unveiling the internal entanglement structure of the Kondo singlet, *Phys. Rev. B* **95**, 115106 (2017).
- [55] R. Zheng, R. He, and Z. Lu, Natural orbitals renormalization group approach to a Kondo singlet, *Sci. China Phys. Mech. Astron.* **63**, 297411 (2020).
- [56] M. Debertolis, S. Florens, and I. Snyman, Few-body nature of Kondo correlated ground states, *Phys. Rev. B* **103**, 235166 (2021).
- [57] S. R. White, Density matrix formulation for quantum renormalization groups, *Phys. Rev. Lett.* **69**, 2863 (1992).
- [58] ITensor Library, <http://itensor.org>.
- [59] M. Fishman, S. R. White, and E. M. Stoudenmire, The ITensor software library for tensor network calculations, *SciPost Phys. Codebases* **4** (2022).
- [60] DMRGpy library, <https://github.com/joselado/dmrgpy>.
- [61] Code and data of the work available in <https://doi.org/10.5281/zenodo.10090477>.
- [62] For edge sites, the average is replaced for the single existing  $n$ th neighbor.
- [63] I. T. Jolliffe and J. Cadima, Principal component analysis: A review and recent developments, *Philos. Trans. R. Soc. A* **374**, 20150202 (2016).
- [64] T. Daimon, Box–Cox transformation, in *International Encyclopedia of Statistical Science*, edited by M. Lovric (Springer, Berlin, 2011), pp. 176–178.